Field survey assessment of flood loads and related building damage from the July 2021 event in the Ahr Valley (Germany)

Wüthrich, Davide; Korswagen, Paul A.; Selvam, Harish; Oetjen, Jan; Bricker, Jeremy; Schüttrumpf, Holger

DOI
10.1111/jfr3.13024

Publication date
2024

Document Version
Final published version

Published in
Journal of Flood Risk Management

Received: 8 May 2023 | Revised: 25 April 2024 | Accepted: 24 June 2024

DOI: 10.1111/jfr3.13024

SPECIAL ISSUE PAPER

CIWEM Chartered Institution of Water and Environmental Management | Journal of Flood Risk Management | WILEY

Field survey assessment of flood loads and related building damage from the July 2021 event in the Ahr Valley (Germany)

Davide Wüthrich[1] | **Paul A. Korswagen**[2] | **Harish Selvam**[3] | **Jan Oetjen**[3,4] | **Jeremy Bricker**[1,5] | **Holger Schüttrumpf**[3]

[1]Department of Hydraulic Engineering, Faculty of Civil Engineering and Geosciences, Delft University of Technology, The Netherlands

[2]Department of Materials, Mechanics, Management & Design, Faculty of Civil Engineering and Geosciences, Delft University of Technology, The Netherlands

[3]Institute of Hydraulic Engineering and Water Resources Management, RWTH Aachen University, Germany

[4]Bezirksregierung Düsseldorf, Düsseldorf, Germany

[5]Department of Civil and Environmental Engineering, University of Michigan, Ann Arbor, Michigan, USA

Correspondence
Harish Selvam, Institute of Hydraulic Engineering and Water Resources Management, RWTH Aachen University, Germany.
Email: selvam@iww.rwth-aachen.de

Funding information
Deutsche Forschungsgemeinschaft, Grant/Award Number: DFG Schu 1054/26-1; TKI Delta Technology, Grant/Award Number: TU02

Abstract

The July 2021 flood heavily affected many inhabitants, buildings and critical infrastructure throughout Germany, Belgium and the Netherlands. Specifically, the Ahr Valley (Germany) showcased the destructive power associated with these extreme events. Hence, this region was the focus of a field survey, aiming at describing the flood-induced damage to buildings and assessing the possible underlying processes that led to structural failures. The field assessment revealed a close connection between building failures and (1) local flow depths and velocities, (2) building location, (3) distance from the riverbank and (4) construction type. Although it is difficult to identify the exact causes that induced failures, the detailed assessment revealed that damages mainly originated from local scour and hydraulic loads, often unevenly distributed around buildings. Importantly, many buildings were significantly affected by (large) floating debris impacts and damming, both responsible for additional loads, highlighting their importance in flood-resistant building design. Furthermore, data showed that buildings near the riverbanks and in the upstream part of villages were more severely damaged. Altogether, data provide a better understanding of the flood processes that lead to building failures, fostering future research towards the development of safer protection measures and more effective flood risk management strategies.

KEYWORDS

disaster recovery, extreme flood events, field survey, flood damages, hydraulic engineering

1 | INTRODUCTION

Floods represent a large worldwide threat, particularly to those communities living within low-lying floodplains. For the 21st century, the estimated number of fatalities connected to river or flash floods is about 7,000,000 people (Merz et al., 2021; UNDRR, 2015) and with an expected global temperature increase of 1.5°C, this number is expected to rise by about 70%–83%, with direct flood losses increasing by 160%–240% through 2050

(Dottori et al., 2018; Merz et al., 2021). Moreover, there are anticipated alterations in the return period of severe floods, including Kundzewicz et al. (2018) and Blöschl et al. (2019), who calculated that floods in north-western Europe previously associated with recurrence intervals of 100 years in 1960 now have intervals of 50–80 years. Contrarily, increased return intervals were found in Eastern Europe, where 100-year flood discharges have now become 125- to 250-year floods. According to Merz et al. (2021), 2500 disastrous floods[1] were recorded worldwide between 1976 and 2005, showing the importance of flood-related research. Major previous events in Germany include the 2002 flood in Saxony (river Mulde) and the 2016 flash flood in Braunsbach, both responsible for heavy structural damage to buildings and critical infrastructure (Laudan et al., 2017).

Most recently, the July 2021 event in North Rhine–Westphalia and Rhineland–Palatinate (Figure 1) led to destructive flash floods caused by intense rainfall over highly saturated soils (Junghänel et al., 2021). This July 2021 flood was a consequence of a high-pressure systems over the Atlantic Ocean and Eastern Europe, accompanied by an intense low-pressure system '*Bernd*' over Central Europe (CEDIM, 2021). The atmospheric moisture held a large amount of precipitable water which was released due to the interaction between high- and low-pressure systems. This resulted in rainfall up to 150–200 mm in 48 h, leading to floods further amplified by the nearly saturated soil from the long-lasting rainfalls of the previous months (CEDIM, 2021). To date, no exact measurement of discharges or flow depths are available since many gauging stations failed during the flood. However, it is believed that the precipitation doubled its monthly average. For example, at measurement gauges in Cologne-Stammheim and Schneifelforsthaus, such high precipitations had never been measured since the beginning of the data record (70 years) and partly exceeded the value of a one-in-hundred-year event. Further detailes on the event's meteorological development can be found in CEDIM (2021). Altogether, this flood caused at least 184 fatalities and injured 820 people (CEDIM, 2021; Thieken et al., 2023), and the resulting destruction of buildings and infrastructure will take years to fix. According to Koks et al. (2022), the economic losses amount to approximately €33 billion. Munich Re (2022) even estimates the economic losses at €46 billion.

The scope of the present study is to present first-hand and reliable field observations collected during the post-

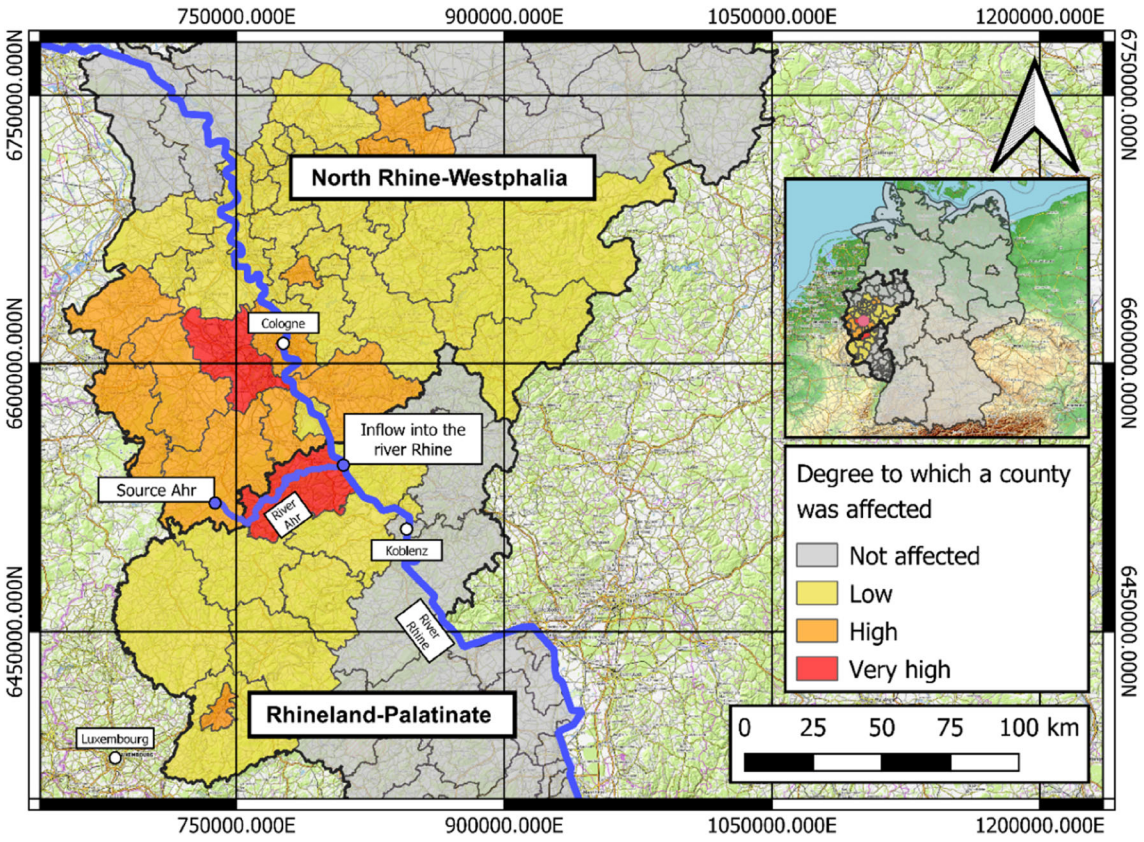

FIGURE 1 Affected areas during the July 2021 flood in Germany. Low = Areas with at least one local flood. High = Areas with extensive flooding and a large number of damaged buildings and/or single fatalities. Very high = Extreme local devastation, many destroyed buildings and/or fatalities (CEDIM, 2021, reworked; Basemap: OpenTopoMap, 2021).

event field survey in the Ahr Valley (Germany) and to describe the flood-induced building damage, assessing the possible underlying processes. The study does not provide an in-depth analysis of the hydrodynamic or mechanical damage processes since the local situation during the field study did not facilitate detailed investigations and measurements. Furthermore, the field study was conducted approximately 1 month after the flood event and while the highly destructive impact was still evident, conditions had already been significantly altered by reconstruction and safety work. Despite these limitations, the field study provided a unique opportunity to investigate the effects of the July 2021 flood on buildings and to collect supporting information from residents (e.g., regarding the chronology of the flood event or details on damaged buildings). This information is summarised and scientifically processed in the present study, where hydraulic/hydrodynamic processes are, if scientifically admissible, briefly assessed.

2 | DATA AND METHODS

2.1 | Study area 'Ahr Valley' (Germany)

An extremely (and probably the most) affected area during the summer 2021 flood is the 'Ahr Valley', at the border between North Rhine–Westphalia and Rhineland–Palatinate (Bung, 2021; Figure 2), which is the focus of this research. The Ahr has a length of 86 km (total catchment area of the River Ahr is 897.5 km^2; MKUEM, 2023), and the valley resembles a notched valley of varying steepness, which fans out in the eastern direction before flowing into the Rhine. The flanks of the valley are often forested and consist of several protected reserves.

During summer 2021, the peak discharge in the Ahr River likely occurred in the late evening of July 14th or early 15th, though the exact time is not known due to failed measurement stations (CEDIM, 2021). For the same reason, it is difficult to determine the end of the event, but on July 17th water levels fell significantly. In '*normal*' conditions, the Ahr is a relatively small river, with a mean discharge of 6.95 m^3/s at Altenahr and a flow depth of 0.75 m. Historical maxima reveal discharges of 236 m^3/s and flow depths of 3.71 m, but according to first estimates, during summer 2021, these values were exceeded by 170–470 m^3/s and 3.3–4.3 m, respectively, leading to discharges up to 400–700 m^3/s and water depths of 7–8 m (CEDIM, 2021).

In the past, the Ahr Valley was affected by many significant floods, including in 1804, 1888, 1910, 1918 and 1920. These were evaluated and quantified by Roggenkamp and Herget (2014) based on historic flood level

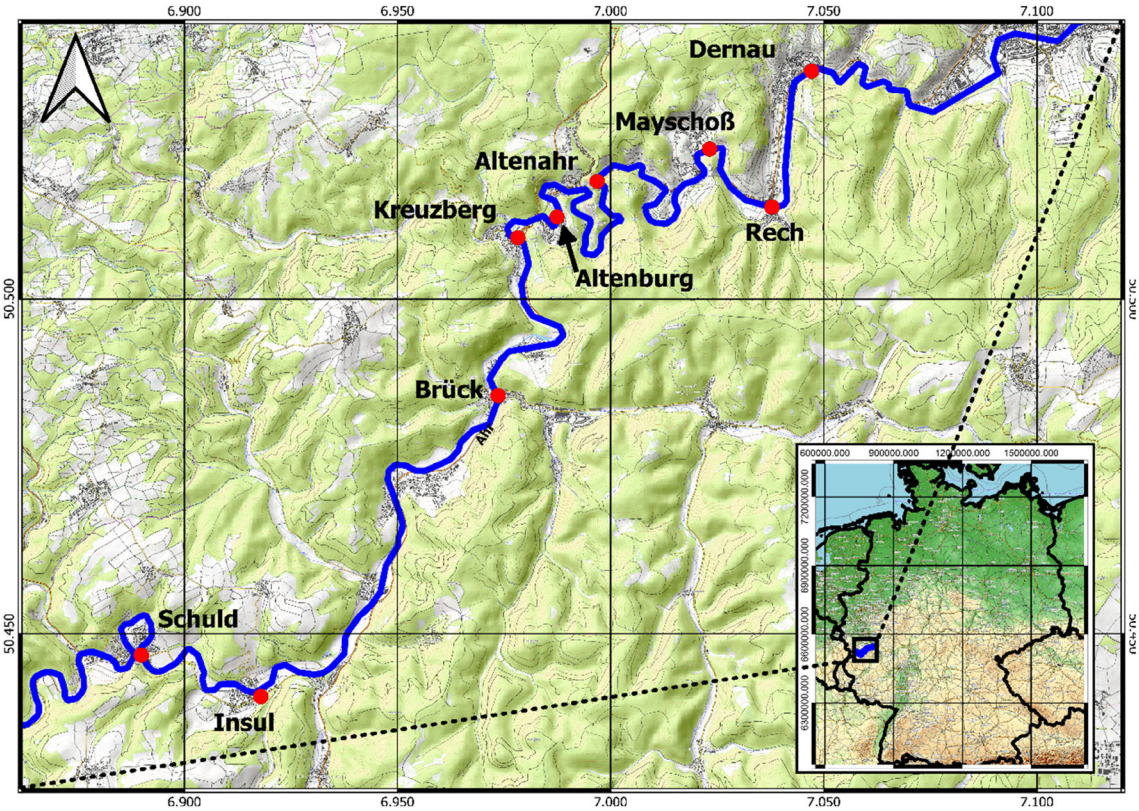

FIGURE 2 Locations within the Ahr Valley investigated in the present report (Basemap: OpenTopoMap, 2021).

markings in Dernau, Walporzheim and Ahrweiler and on photographs taken in Neuenahr in 1910. Most information is available for the 1910 event, which posed great danger to residents and damaged many buildings and bridges along the River Ahr (Roggenkamp & Herget, 2014; Ulrich, 1938). The flood event in 2021 is believed to have been less intense than the event in 1804 but comparable to the event in 1910 (CEDIM, 2021), however, land uses have evolved throughout the years, which hinders any direct comparisons between flood events.

Despite their large magnitude, the 1804 and 1910 events are currently not considered in the official risk assessments for the Ahr Valley since these are based on measurements beginning in 1947. Without these major floods, the estimate for a flood event HQ_{100} (i.e., one-hundred-year estimate) was determined to be 241 m^3/s (CEDIM, 2021). However, analyses performed by Vorogushyn et al. (2022) show that it is important to consider all historical events (e.g., 1804 and 1910). With these, they calculated a recurrence interval of 8600 years for the 2021 flood event, while their calculations resulted in recurrence intervals of >100 million years when historical events were not considered. Roggenkamp and Herget (2022) assessed the maximum discharges along the Ahr by relating water-level marks to measurements of flooded cross-sections, slope and roughness, calculating a '*new*' maximum flood discharge of 645 m^3/s downstream of Müsch (previous $HQ_{100} = 152\ m^3/s$) and 1230 m^3/s downstream of Rech. These values are only estimates since the accuracy of the watermarks is questionable (Roggenkamp & Herget, 2022), but they clearly show the intensity of this flood compared to previous historical events, proving its catastrophic nature and scientific relevance.

2.2 | Field survey methodology

Field surveys are a fundamental tool to better understand the physical behaviour of these extreme events, and many were conducted after tsunamis, floods, earthquakes and hurricanes (e.g. Chock et al., 2013; Widiyanto et al., 2019; Paulik et al., 2021).

The Ahr Valley field survey was conducted by a team of researchers from TU Delft and RWTH Aachen University on 17–19 August 2021. The post-event field survey covered 12 locations along a stretch of ~30 km of the Ahr Valley, as shown in Figure 2. Surveyed villages included Marienthal (furthest downstream), Dernau, Rech, Mayschoß, Altenahr, Altenburg, Kreuzberg, Ahrbrück, Honningen, Liers, Insel and Schuld (furthest upstream). Over the 3 days, the field survey collected various geo-referenced pictures (Canon 6Dii with standalone GPS log) as well as measurements of structural damages and water levels using both manual rulers and laser rangefinders (Leica Disto D3-LV1). The field survey also included discussions with local inhabitants, who voluntarily approached the survey team and kindly shared their first-hand experiences during the flood events. A preliminary fact-finding overview of these data can be found in Korswagen et al. (2022), while additional survey data can also be found in the independent study of Maiwald et al. (2022).

In particular, this field survey focused on the following aspects to analyse the flood actions imparted on buildings and their associated failure mechanisms:

1. Water depths, measured from watermarks left on buildings façades (Section 3);
2. Local scour at selected building locations and bank erosion, with a specific interest on their implication on building stability (Section 4.1);
3. Building damages, with the objective of reconstructing the most common failure mechanisms that occurred during the flood (Sections 4.2 and 4.3).

It is important to mention that the estimation of discharges and flow depths was not part of the present study, for which indicative values are provided in the introduction. However, since water levels and local flow conditions highly affected the loading and failure mechanisms within the flooded area, local water levels at building locations were recorded during the survey, and a brief overview is presented hereafter.

3 | WATER DEPTHS

The water marks left by the flood were still visible on the façades of multiple buildings, and a dataset of maximum water depths was collected at different locations. These were measured as the distance from the ground to the watermark on the structure, and their range is summarised in Table 1.[2] Data were collected for buildings that were within a 100 m distance from the river.

Data showed a large variability of water depths throughout the Ahr Valley, with some villages revealing values substantially higher than others. In particular, the highest values were observed in Altenahr, where water depths exceeded 7 m for the houses closer to the river, while the lowest ones were recorded in Liers and Honningen, with values of 1.4–1.5 m. Such variability is likely associated with: (1) the topography of the region and (2) the local hydrodynamic conditions of the flow during the flood. In particular, the narrow portions of the valley

induced higher water depths, while larger floodplains contributed to the lower values. In addition, field observations revealed that extrados (outside) of river bends were often associated with higher water depths, with implications on scour, bank erosion and hydrodynamic loads discussed in Section 4.

TABLE 1 Range of local water depths in the Ahr Valley investigated during the survey.

Village	Distance from river mouth	Number of investigated buildings	Water depth
Schuld	51.4 km	10	1.9–3.7 m
Insul	47.4 km	3	1.7–3.3 m
Liers	43.8 km	2	1.5–1.6 m
Honningen	41.4 km	1	1.4 m
Ahrbrück	38.7 km	3	2.7–3.3 m
Kreuzberg	34.7 km	9	2.2–3.8 m
Altenburg	33.5 km	5	5.2–5.7 m
Altenahr	32.0 km	7	4.0–7.2 m
Mayschoß	30.2 km	2	2.5–4.2 m
Rech	22.8 km	1	3.8 m (~1/3 of first floor)
Dernau	20.0 km	5	3.0–4.3 m
Marienthal	18.7 km	4	4.1–5.5 m

Spatial variability of the water depths was also associated with the local hydrodynamic behaviour of the flood. In particular, it was noted in several buildings that the distribution of the water marks was uneven around the four sides, as shown in Figure 3. For instance, a house in Altenahr (Figure 3c) showed a water depth of ~4.9 m on the downstream side, while the corner on the upstream side revealed marks up to 5.7 m. This corresponded to a ratio of 1.16, which is slightly higher than previous laboratory observations for steady flows around buildings with various geometries by Wüthrich, Pfister, et al. (2020). Similar results were also observed in Schuld, where a building in the centre of the village showed that a façade frontally exposed to the flow showed water marks at 3.0 m, while the sides had marks at 2.1 m (Figure 3e). This showed a ratio between the front and side of 1.4, which was higher than the house in Altenahr, thus suggesting a slightly high velocity flow. These data confirmed the spatial variability of the flow conditions during the flood, as well as the non-uniform distribution of loads acting on buildings, further addressed in Section 4.

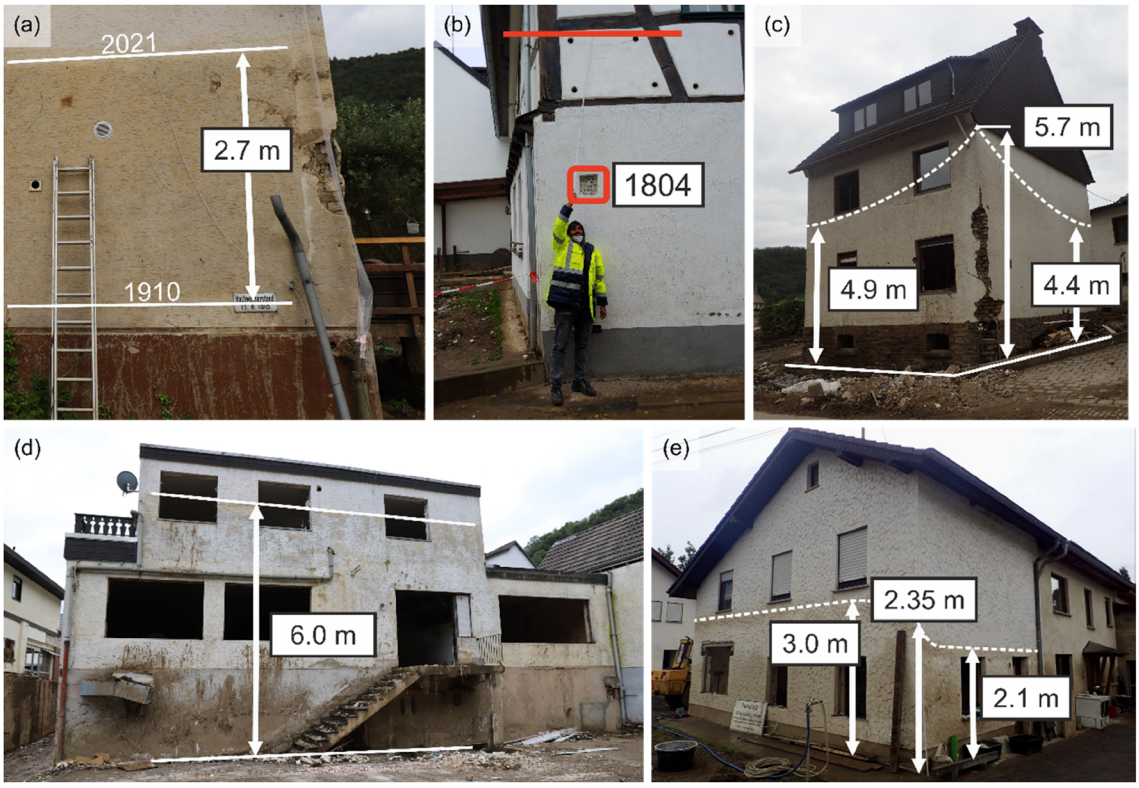

FIGURE 3 Watermarks in the Ahr Valley: (a) Ahrbrück; (b) Walporzheim; (c) Altenahr; (d) Altenahr; (e) Schuld; (c) and (e) have a non-uniform distribution of water marks on buildings during floods; (a) provides a comparison of the 2021 flood with the extreme event of 13 June 1910, while (b) shows the difference between the 1804 and 2021 floods.

FIGURE 4 Scour at various buildings corners in: (a) Schuld; (b) Altenahr; (c) Marienthal.

4 | BUILDING FAILURES

At the time of the survey, many buildings exhibited partial or total (structural) failure. This section describes the flood actions and the context that led to these failures, with the goal of furthering the understanding of floods' effects on buildings. This will support the development of effective strategies to mitigate flood actions and to improve flood risk management. First, flood actions affecting buildings through their foundations are considered (Section 4.1), followed by the hydro-static and hydrodynamic forces on buildings (Section 4.2); finally, the effect of debris is discussed (Section 4.3).

4.1 | Failures due to scour and bank erosion

4.1.1 | Scour around buildings

Buildings in flooded areas change the flow dynamics, inducing strong fluid–structure interaction phenomena that result in local vortices around buildings. These vortices are often responsible for the removal of soil from the foundation when the external stresses applied by the flow are greater than the critical stresses required to trigger the motion of soil particles (Kohli & Hager, 2001; Melville, 1997). During the field survey, many locations revealed local scour at buildings' corners (Figure 4), where acceleration and flow separation occurred. These local changes increased the flow velocity, turbulence intensity and bed shear stresses, altogether responsible for the scour. In addition, most buildings affected by scour were shown to be either adjacent to the river or had more complicated geometries that protruded outside of the rectangular layout. A summary of observed scour is presented in Table 2.

Nevertheless, it was observed that in most cases, the scour at the corners did not affect the building's stability since it was not deep enough to reach the foundation (Figure 4). However, the spatial variation of the depth of the scour holes also confirmed the uneven distribution of pressures and increased flood loads on buildings (ASCE 7, 2017; FEMA, 2007), as shown in Section 4.2. For shallow slab or strip foundations, in some cases, the scour depth exceeded the foundation depth (Figure 5). Thus, once the scour reached the foundation, the continuous high-velocity flow likely started undermining the soil under the foundation slab, resulting in an overhanging or a partially supported slab. Nevertheless, the buildings remained stable despite the flood heavily damaging the upper timber storey (Figure 5b).

At a few locations, the scour occurred at the front of the building, where the upstream recirculation dug a large amount of material, with a comparatively smaller soil removal along the sides (Figure 6). This pattern aligns with the experimental observation of tsunamis interacting with squared buildings (see figs. 7 and 11 in Mehrzad et al., 2022). This type of scour was found in front of buildings that are un-sheltered (or partially sheltered) by upstream elements, and this pattern is known to depend on the ratio between building width and flow

depth (Kohli & Hager, 2001; Melville, 1997). Physically, the incoming flood water, obstructed by the presence of the building, deviates around the structure, accelerating and creating a horseshoe vortex responsible for the removal of a significant portion of soil (Lee & Hong, 2019; Melville & Raudkivi, 1977; Unger & Hager, 2006) (Figure 6). These horseshoe and lee-wake vortices often exposed support piles, thus confirming the intensity of the flood throughout the Ahr Valley.

During the inspection, scour depths of 0.5–1.5 m were frequently observed at building corners, with scour lengths ranging from 1.5 m to 2.5 m (Table 2). Further attempts were made to compare these values with existing empirical equations. For that, the bridge pier equation reported by Richardson and Davis (2001) and Arneson et al. (2012) in HEC-18 ('*Evaluating scour at Bridges*') is used, similar to the approach of Bricker et al. (2012) for tsunami-induced scour. Flow parameters (velocity and flow depth) were obtained from the numerical simulations of Apel et al. (2022), while the soil parameters were based on field investigations by another field survey team from RWTH Aachen of a nearby site. The field investigation revealed that the upper layer of the soil was cohesive, with d_{50} ranging between 0.012 and 0.036 mm. Since Apel et al. (2022) only covered certain regions within the Ahr Valley, the comparison was only conducted for S1 and S2 (shaded in grey in Table 2). Detailed scour calculations are given in the Supporting Information Material (see online version of this article), while the main results are summarised in Table 3.

Results showed that despite the width correction factor, the pier scour formula (eq. 6.1 in Richardson & Davis, 2001) over-predicted the measured scour at both locations by 1.9 and 3.8 times, respectively. Similarly, the abutment formula (eq. 7.1 in Richardson & Davis, 2001) over-predicted the measured scour by 3.6

TABLE 2 Scour depths measured at selected locations during the survey.

Name	Address		Figure No.	Latitude	Longitude	Scour depth (m)	Scour length (m)	Scour location
	Location	Street						
S1	Marienthal	Marienthal Straße	4d	50.53256	7.062555	1.25	1.5	Corner
S2	Marienthal	Im Guten Acker	6c and 6d	50.53477	7.056537	1.20	–	Around the building
S3	Kreuzberger	Am Brunnen Straße	4b	50.51064	6.979071	0.75	2.5	Corner
S4	Altenahr	Seilbahnstraße	4c	50.51586	6.985633	1.30	2.5	Two corners
S5	Brück	Ahrstrasse	5	50.4833	6.972411	1.20	–	Corner
S6	Brück	Ahrstrasse	6a and 6b	50.48315	6.971483	1.25	–	Front
S7	Insul	Klaustrasse	–	50.44177	6.916729	1.50	-	Front
S8	Insul	Brückenstraße	–	50.44241	6.915654	0.45	-	Corner; interior building
S9	Schuld	Ahrstrasse	4a	50.44666	6.886958	0.40	2.5	Corner

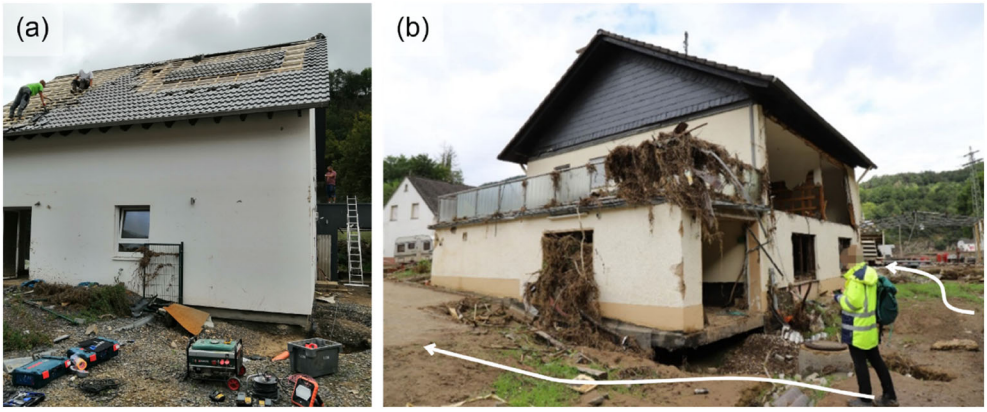

FIGURE 5 Damaged building in (a) Kreuzberg and (b) Brück, where scour at the corner reached the foundation. In (b) debris accumulation can also be observed.

FIGURE 6 Examples of scour around buildings due to the formation of horseshoe vortex. Figures (a) and (b) were taken in Brück (same building, front and side view), Figures (c) and (d) were taken in Marienthal with (d) and (e) showing scour protection by block pavement; Figure (e) was taken in Kreuzberg.

TABLE 3 Measured and calculated scour depths at two locations in Marienthal (S1 and S2 are defined in Table 2).

	Scour at S1 (m)	Scour at S2 (m)
Measured scour depth	1.25	1.20
Pier equation (Section A.1)	2.38	4.59
Abutment equation (Section A.2)	4.50	6.81
Pier equation for cohesive soil (Section A.3)	0.52	1.18

and 5.7 times, respectively. A possible explanation is that the scour did not reach equilibrium during the flood since the soil was cohesive (Li et al., 2002; Sonia Devi & Barbhuiya, 2017). Hence, Arneson et al. (2012) introduced a formulation for cohesive soils utilising Briaud et al. (2011) (eq. 7.35 in Arneson et al., 2012), which includes time-dependency. These predictions are more aligned with measurements at S2, with an underestimation at S1, probably due to an under-prediction of the local flow velocity in the numerical simulations and/or the presence of small vegetation and rubble mounds around the buildings. These simple calculations pointed out the lack of precise formulae for predicting building scour during flash floods in cohesive soils, revealing the need for further research.

Overall, the development of scour highly depends on the local soil characteristics (e.g., porosity, saturation, pore pressure, etc.), flow conditions and the possible presence of protection measures (Hager & Unger, 2010; Kohli & Hager, 2001; Krautwald et al., 2021). Furthermore, the development of maximum scour depth at any location is time-dependant (Hager & Unger, 2010; Kothayari et al., 1992; Melville, 1997; Zevenbergen et al., 2004). Field observation also demonstrated that

buildings adjacent to the river (Figure 4c), at the end of streets (Figure 4a,b) or with protrusions outside of the regular rectangular layout (Figure 5a) experienced more intense scour at corners, whereas buildings that were not sheltered experienced large scour at the front (Figure 6a,b). Thus, the intensity of the scour can be partially related to the building location with respect to the direction of the flow. This confirms the need for further research on scour generating processes and on the vulnerability of buildings to scour, accounting for the spatial variability within a village and irregularity in buildings shape.

Figure 6d shows a building on the Marienthal flood plain, where scour would be expected, in line with neighbouring buildings. However, observations revealed no scour-hole around this building, where block pavements likely prevented soil removal. Similar observations were made at several locations (e.g., Figure 6e). Although the pavements were partially broken at a few sites, they still protected the buildings against scour and served as a first layer of protection. The use of revetments for scour and riverbank protection is not new, and deep-routed grass and block pavements have been widely suggested in the past (Gray & Barker, 2004; Julien, 2002). However, these field observations confirmed the effectiveness of these scour protection measures during floods, stressing their importance for flood protection and risk mitigation.

4.1.2 | Failures related to bank erosion

Buildings adjacent to the river suffered largely from bank erosion. The sustained water levels and high velocities removed a significant portion of the river bank, which could not be prevented despite the protection with natural vegetation, including grass and trees (Abernethy & Rutherfurd, 1998; Gray & Barker, 2004). Locals reported that after the flood the river had doubled its regular width at many locations. In addition, bank erosion reached many buildings adjacent to the river, compromising their foundations. Since most buildings in the Ahr Valley have one or two storeys, the common type of foundation observed was shallow foundation,[3] including isolated footings, strip footings or slabs. Shallow foundations transfer building loads to the earth near the surface rather than deeper soil or rock strata. This means that bank erosion often daylighted these shallow foundations, resulting in sizeable structural failures. A typical example is shown in Figure 7b, where a concrete strip footing of approximately 1.2 m was exposed below the basement, triggering the failure of part of the building (Korswagen et al., 2022). Note that despite the grass protection, the bank erosion extended inland for approximately 8.6 m, based on pre-event satellite imagery on 24 March 2020. This confirms, once again, the importance of reliable bank protection measures, particularly for heritage buildings near the river.

Field observations showed that bank erosion intensified at extrados (outside) of river bends and where the flow was obstructed. Studies by Wu and Molinas (2005) showed that a significant obstruction of the flow (e.g., bridge piers) can trigger a choked flow regime, resulting in higher upstream water levels and higher flow velocities around piers. One example was found in Rech, where the upstream bridge obstructed the flow (Figure 8), probably increasing the downstream flow velocity and resulting in considerable bank erosion with the collapse of one pier (Figure 8c). The building in Figure 8b was constructed at the extrados of the river bend, and the exposure of its simple-footing foundation due to bank erosion prevented any load transfer to the soil. The lack of support for the overhanging part of the superstructure led to the failure of both structural and non-structural members, emphasising the need for deeper foundations near riverbanks. According to BMUB (*German Federal Ministry for the Environment, Nature Conservation, Nuclear Safety and Consumer Protection*), building foundations should be at least 1 m below the expected erosion and scour depth. Preferably, shallow foundations should be replaced with pile foundations in future constructions, especially for buildings near river bends and in proximity of bridges. Furthermore, it is worth mentioning that bridge piers and abutments were also affected by scour at many locations (Figure 8c).

During the survey, some bank erosion at the intrados (inside) of river bends was also observed, also affecting building stability. The example in Figure 9 revealed an eroded depth of around 1.5–1.8 m, exposing the shallow foundation (square columns) of the building. However, the footing remained grounded, ensuring the stability of the building, contrary to Figure 8b.

Overall, these observations pointed out the critical role of reliable building foundations in limiting damage, particularly for structures near riverbanks, where erosion effects should be of primary importance during the design process. Furthermore, failures were more frequent in areas without hard protection measures (e.g., gabions and rip-rap revetments), while natural bank protection measures (e.g., grass and vegetation) were shown to be insufficient during extreme floods (Zhu et al., 2018).

4.2 | Failures due to hydrostatic and hydrodynamic loads

Floods exert hydrostatic and hydrodynamic loads on buildings. The former are the result of a water-level difference between the inside and the outside, while the

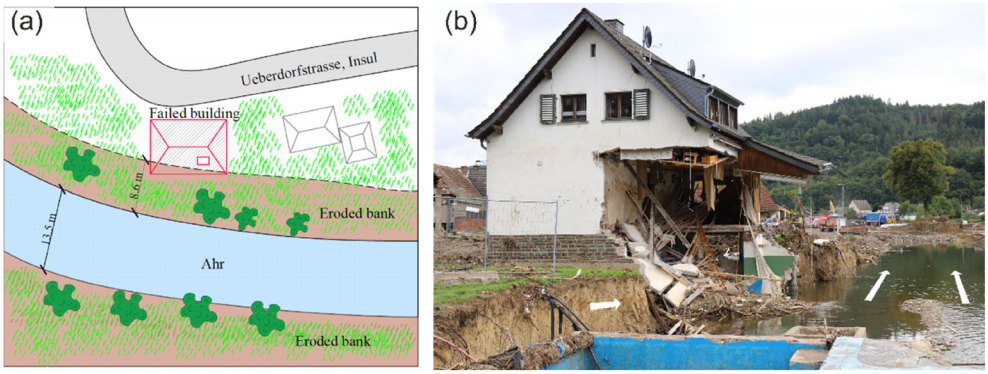

FIGURE 7 Bank erosion-related failure in Insul. Sketch (a) is based on satellite imagery from Google Earth on 24 March 2020; (b) image taken during the suvery.

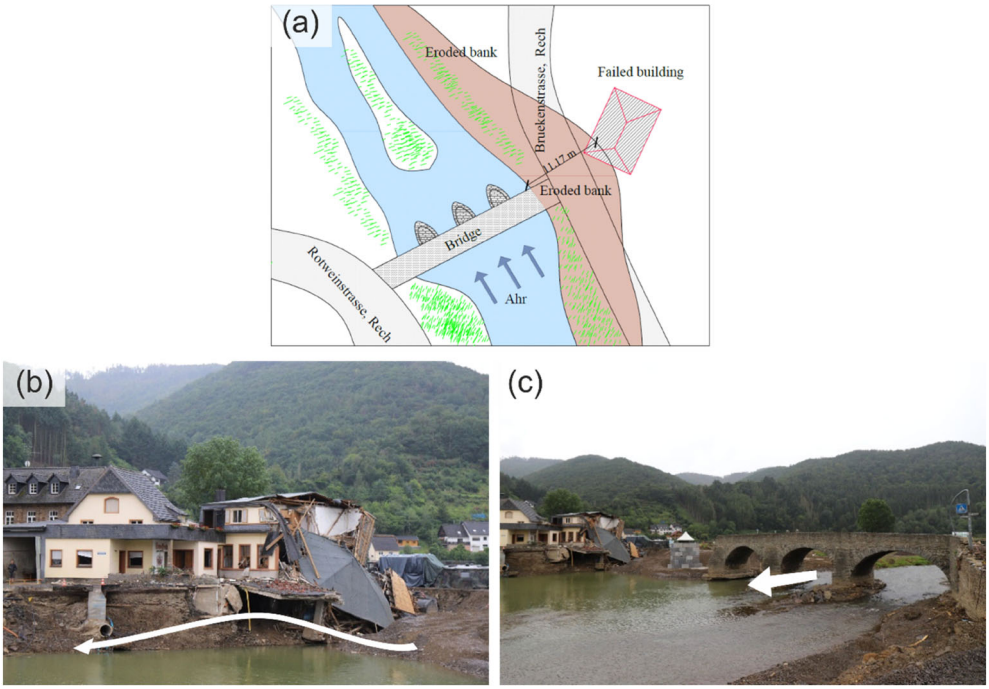

FIGURE 8 Bank erosion related failure in Rech at the extrados (outside) of river bend due to flow obstruction of the upstream bridge. Sketch (a) is based on satellite imagery from Google Earth on 24 March 2020.

latter are associated with moving water (Cantelmo & Cuomo, 2021; Jansen et al., 2020; Kelman & Spence, 2004; Nadal et al., 2010). Often during floods, water can enter buildings, reducing the water-level difference between inside and outside, and therefore neutralising the hydrostatic load. However, hydrodynamic loads still occur for considerable flow velocities.

Field observations showed several masonry, timber and half-timbered buildings, the latter made of traditional German vernacular architecture consisting of heavy timber posts, beams and braces left exposed and infilled with plastered wattle or other infill materials, as depicted in Figure 10a,b. These types of buildings suffered significant damage associated with hydrostatic and hydrodynamic loading; at several locations, the structural damage level ranged from moderate (D3) to heavy (D4), as classified by Maiwald and Schwarz (2015). The high flood levels during the 2021 event heavily damaged buildings façades, even reaching the first floor at many locations. In particular, it was noted that the failure of façades significantly altered the structural integrity of old, unreinforced (fired-clay) masonry buildings (damage grade D4). In contrast, modern concrete constructions were able to sustain higher water levels, e.g. in Altenahr and Altenburg where measurements showed depths of 5–7 m. While these structures did not experience any structural damage, the flood was still responsible for the failure of windows and doors, associated with a damage grade D2 (Figures 3d and 10c). These observations comply with Schwarz and Maiwald (2007) and Maiwald and Schwarz (2015) after the 2002 floods in Saxony. The study reported that the damage is intrinsically linked to the flow-action parameters (i.e., inundation level, flow velocity and specific energy) and resistance of the building (e.g., type of construction, building type and conditions). Thus, flood-resistant buildings such as modern

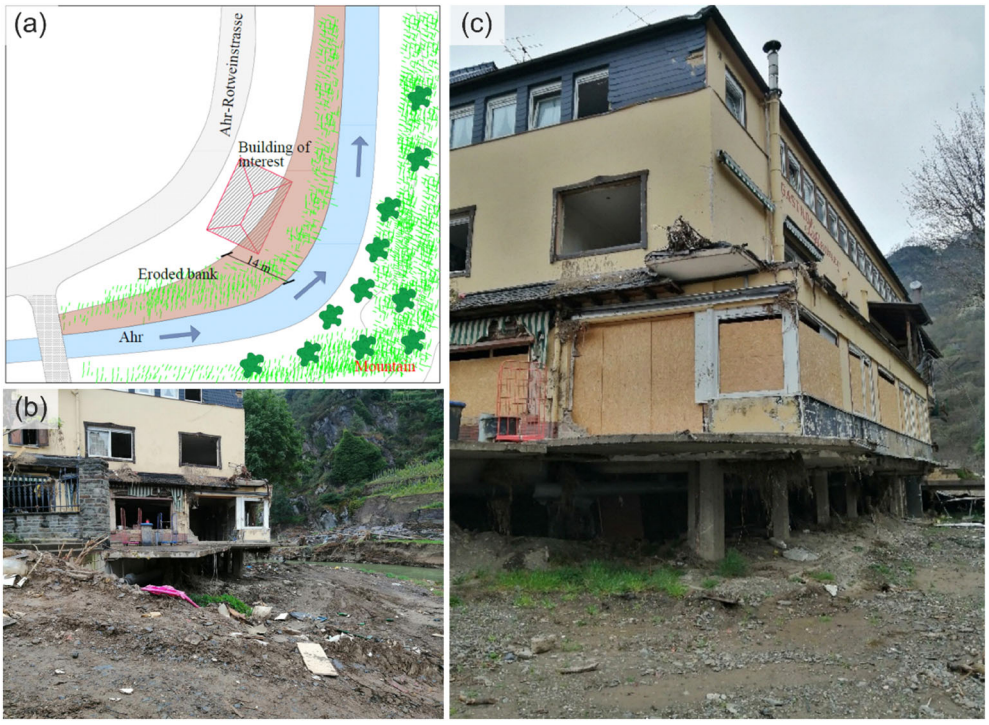

FIGURE 9 Bank erosion at the intrados (inside) of the river bend in Mayschoß. Sketch (a) is based on satellite imagery from Google Earth on 24 March 2020. Please note that photo (b) was taken on 17 August 2021, whilst photo (c) on 30 March 2022.

FIGURE 10 Failure of traditional half-timbered structures due to flood loading in Schuld (a) and in Kreuzberg (b) while (c) shows a modern construction in Altenahr, with a concrete structure that sustained flood loading.

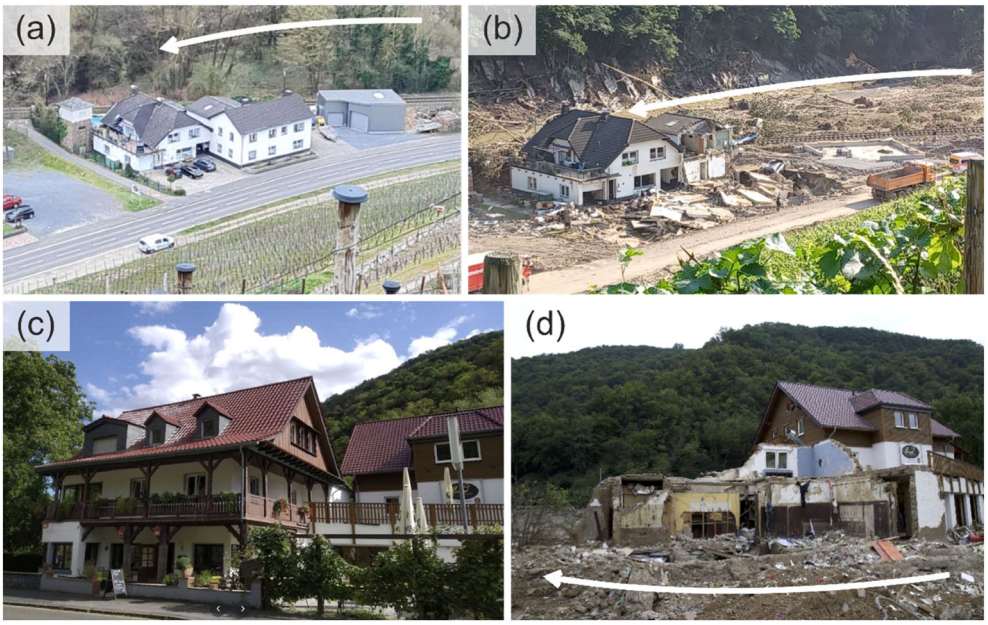

FIGURE 11 Figures (a, b) show a failure due to buoyancy and horizontal loads in Marienthal, and the floor plan layout; (a) before flood; (b) after the flood. Figures (c, d) show the failure of the L-shaped floor plan layout; (c) before flood; (d) after the flood [*Source*: (a, b) Photographs by Moni Körtgen, house owner. (c) Google photos; photo courtesy of Heidi Möller on August 2020. Date accessed: 30 August 2022] (Möller, 2020). Arrows indicate presumed flow direction.

concrete or soft-storey buildings are less vulnerable to floods compared to (half-)timber(ed) and masonry buildings.

A critical load during floods is buoyancy, which tends to uplift and destabilise structures. Many buildings in the Ahr Valley are constructed with timber and lightweight materials, which were particularly affected by the buoyancy-induced vertical loads associated with the high water levels. Figure 11a,b presents an example that occurred to the first '*un-sheltered*' building upstream of Marienthal. An eyewitness reported that part of the building was initially sheared-off from the foundation and turned over by the water. This detachment could be linked to the large buoyancy force resulting from the rapid water level rise, while the movement of the building was likely associated with the strong momentum of the flow. Nevertheless, many buildings sustained the initial buoyancy loads since water entering the structures added weight to the building, inducing a stabilising effect. Such buoyancy effects can be threatening for buildings with large enclosed areas, facilitating uplift. Similar observations were also observed during tsunamis (Chock et al., 2013; Sundar et al., 2007) and in laboratory experiments by Wüthrich et al. (2018) and Harish et al. (2022a, 2022b).

Interestingly, the building in Figure 11a was built with an 'L-shaped' plan, which was severely damaged during the flood. Similar observations were made for other buildings (e.g., Figure 11d), suggesting that the L-shape layout generates large loads at the junction, due to flow accumulation and recirculation (Figure 11a). A specific analysis of pressure distribution for such layouts would be of interest to better understand the physical processes involved.

Openings within buildings in the form of breakable windows and doors could neutralise the hydrostatic pressures and reduce the hydrodynamic load (Wüthrich et al., 2018). However, during the field observation, it was noted that openings and spaces inside buildings were utterly filled with floating debris, including tree branches, plastic, furniture and sediments (Figure 15a). During the flood, these debris accumulated in buildings, shattering the openings and filling the empty spaces, forming '*debris dams*', which resulted in an increased area exposed to floods (Wüthrich, Ylla Arbós, et al. 2020). For this reason, ASCE 7 (2017) recommends that the reduction of design loads due to openings should not exceed 30%, even for buildings with a large opening percentage. Given their relevance, the effect of large floating debris is discussed in Section 4.3.

4.3 | Failures due to floating debris

Multiple objects were transported by the flood and left stranded throughout the Ahr Valley, consisting mainly of tree trunks and broken branches, building components such as roofs, doors, or window frames, (house) tanks for water or heating oil, household appliances and furniture, small cars, bicycles, and motorcycles. This debris affected buildings via two processes: (1) floating debris collided against the structures (Ikeno et al., 2016); (2) debris accumulated around buildings, forming a '*dam*' (Schmocker & Hager, 2013), in line with post-tsunami field observations (e.g., Chock et al., 2013). The type of debris and these two processes, as well as the forces exerted on structures, are discussed next.

FIGURE 12 Damage associated with debris (a) marks on buildings by debris impact (Schuld); (b) debris damming around a building (Dernau).

4.3.1 | Type of debris

The type of debris that may become water-borne or be dragged by a flood depend on (1) debris availability in the region and (2) flood's characteristics. For example, in mountain regions, debris mostly consist of wooden trees and branches from upstream forests (Bezzola & Hegg, 2007). Contrarily, in harbours prone to storms surges or tsunamis, shipping containers are often found (Goseberg et al., 2016). An overview of possible 'drifters' is provided by Bayón et al., (2024). The surveyed region was surrounded by mountains and debris mixtures were observed around structures, collected in piles by emergency response groups, or witnessed by locals. Based on these, the following considerations can be made:

1. Most debris mixtures included wooden logs, trunks of trees, branches, and rootstocks. While the source of these debris remains uncertain, plausible options are: (1) logs lying along the riverbanks; and/or (2) trunks uprooted/broken by the large flow depths and velocities. In addition, large bank erosion exposed rootstocks, which worsened the generation of wooden debris. This emphasises the need for well-maintained riverbanks and floodplains, free of trees and branches, often left untouched for ecological reasons. No detailed quantification of volumes and key characteristics of debris was conducted during the survey, but a qualitative inspection revealed logs of various sizes, with diameters of 30 cm and lengths of 3–6 m being common. Small (<0.5–1 m) woody debris was also observed, which is particularly harmful to buildings due to its interlocking nature. Figure 12b also shows many sediments entrapped upstream of buildings, contributing to the formation of '*debris-dams*'.
2. A significant portion of debris consisted of building rubble, roof structures, doors and window frames, due to damages to upstream buildings. Similarly, household and city appliances such as washing machines, (oil) tanks and furniture were often seen, together with benches and (farm or garden) fences. Additional large floating debris included vehicles such as bicycles, motorcycles, cars, motorhomes and caravans. Altogether, this man-made debris became entangled with the wooden debris (Figure 13), increasing the accumulation volumes.

4.3.2 | Debris impact

Floating debris is transported by the flood, following its direction and speed (Rueben et al., 2015). When the flow encounters an obstacle, including bridges or buildings, the debris redirects sideways, downwards, or penetrates through the building openings. Debris with a high momentum (which hinders rapid changes in direction) or those of considerable size that prevents passage through building openings, collide against the structure, usually at corners or around openings. Figure 14 shows several traces of these collisions, most likely caused by similar and/or repeated events. Observations indicate that most impacts occurred slightly below the watermark, suggesting floating debris were partially submerged or the collisions occurred at flood levels below the maximum water depth. This seems reasonable since lower parts of the building were submerged for a longer time, while the maximum water depth only occurred for a short period.

Figure 3c showcases a debris impact on a building, suggesting that the affected corner corresponded to the most upstream edge. The building also shows small impacts near the window openings on the ground floor. Presumably, repeated collisions progressively dislodged the old concrete masonry units and failure was exacerbated by the flow erosion of the joints, which led to the

FIGURE 13 Various types of debris: (a) cars dragged and rolled by the flood (Dernau); (b.1, b.2) car-sized tank among a large pile of woody debris (Kreuzberg); and (c) several timber items collected in front of a house (Kreuzberg).

observed corner failure. Similarly, Figure 14a depicts a house with an outer veneer of fired-clay brick masonry which failed in the corner, presumably due to the impact of floating debris. The veneer was insufficiently supported by the inner structural walls of concrete blocks and floors; the ties, connecting both leaves of the cavity wall through the air or insulation chamber, are designed to provide stability and withstand wind loads. The examples provided in Figure 14c,d,f present traces of similar debris collisions on buildings edges, while Figure 14g shows additional impacts at window corners on the first storey. Finally, Figure 14e shows a traditional rubble stone masonry building, also revealing a structural failure, likely due to debris impact.

The maximum force of an elastic collision can be described as

$$F = v \times \sqrt{m \times k}, \tag{1}$$

where v is the velocity, m is the mass of the object, and k is the stiffness of the collision dependent on both the stiffness of the debris and of the wall (Nistor et al., 2017). A similar expression is used by ASCE 7-16 Chapter 6 '*Tsunami loads and effects*' (ASCE 7, 2017), where k is the effective stiffness of the impacting debris or the lateral stiffness of the impacted structural element(s) deformed by the impact, whichever is less. Logs and poles are assumed to strike longitudinally, and the stiffness can be calculated as $k = EA/L$, where E is the longitudinal modulus of elasticity of the log, A its cross-sectional area, and L its length. ASCE 7 imposes a minimum log stiffness of 61,300 kN/m and a minimum weight of 454 kg. Wood properties vary widely, but this corresponds approximately to a 9.15 m long with a 30.5 cm diameter (ASCE 7-16 Chapter 6 Commentary). In the Ahr Valley, the value of the diameter aligns with observations, while the length specified by ASCE 7 appears to be on the conservative side, since logs between 3 and 6 m were more frequently found. For completeness, Matsutomi (2009) and Ikeno et al. (2016) refined Equation (1) to include the potential rotation of the impacting debris, drag effects and local damage of woody debris (see also Korswagen, 2016). However, collisions that lead to building damage are better characterised by the energy released during the impact, which cannot be expressed in a simple equation, but can be read from a force–displacement diagram of the wall, generated for the presumed point of impact and accounting for the dynamic effect of the collision.

4.3.3 | Debris damming and accumulation

The high availability of branches, logs, debris and sediments allowed the flood to build *debris-dams* around obstacles. The floating branches and logs tangled with

FIGURE 14 Damage and partial failures caused by the impact of floating debris, below the water-mark. (a) Dernau; (b) Altenahr; (c, d) Kreuzberg; (e) Schuld; (f) Brück; (g) Kreuzberg.

other types of debris, accumulating on the upstream side of buildings and bridges. The water flowed around or through the building openings, allowing the debris-dams to collect additional material and to become larger and more compact. The changing water level also generated debris-dams that grew in height, and the branches trapped additional debris floating past. Post-flood images in Figure 15c,d revealed that some buildings were completely surrounded by debris, hence underlying the importance of this accumulation phenomenon. These debris-dams generated an upstream increase in water level, which led to larger hydrostatic pressures. Large debris-dams also blocked building openings, thus increasing the area exposed to the flood and therefore the total loads transferred to the structure. This was shown in laboratory experiments by Stolle et al. (2018) and Wüthrich, Ylla Arbós, et al. (2020), confirming that woody debris forms a more compact and entangled dam, which blocks the flow more effectively in comparison with other debris, thus leading to a higher backwater effect. This resulting force may be sufficient to cause serious structural damage to the buildings, especially when the *debris-dam* pushes the roof, typically constructed of timber frames. Figure 15 shows locations, where debris around buildings had not yet been removed, visualising potential configurations of these dams. Figure 15e shows the damaged building after the debris was removed. Figure 15d depicts the debris accumulated in front and partly through an opening.

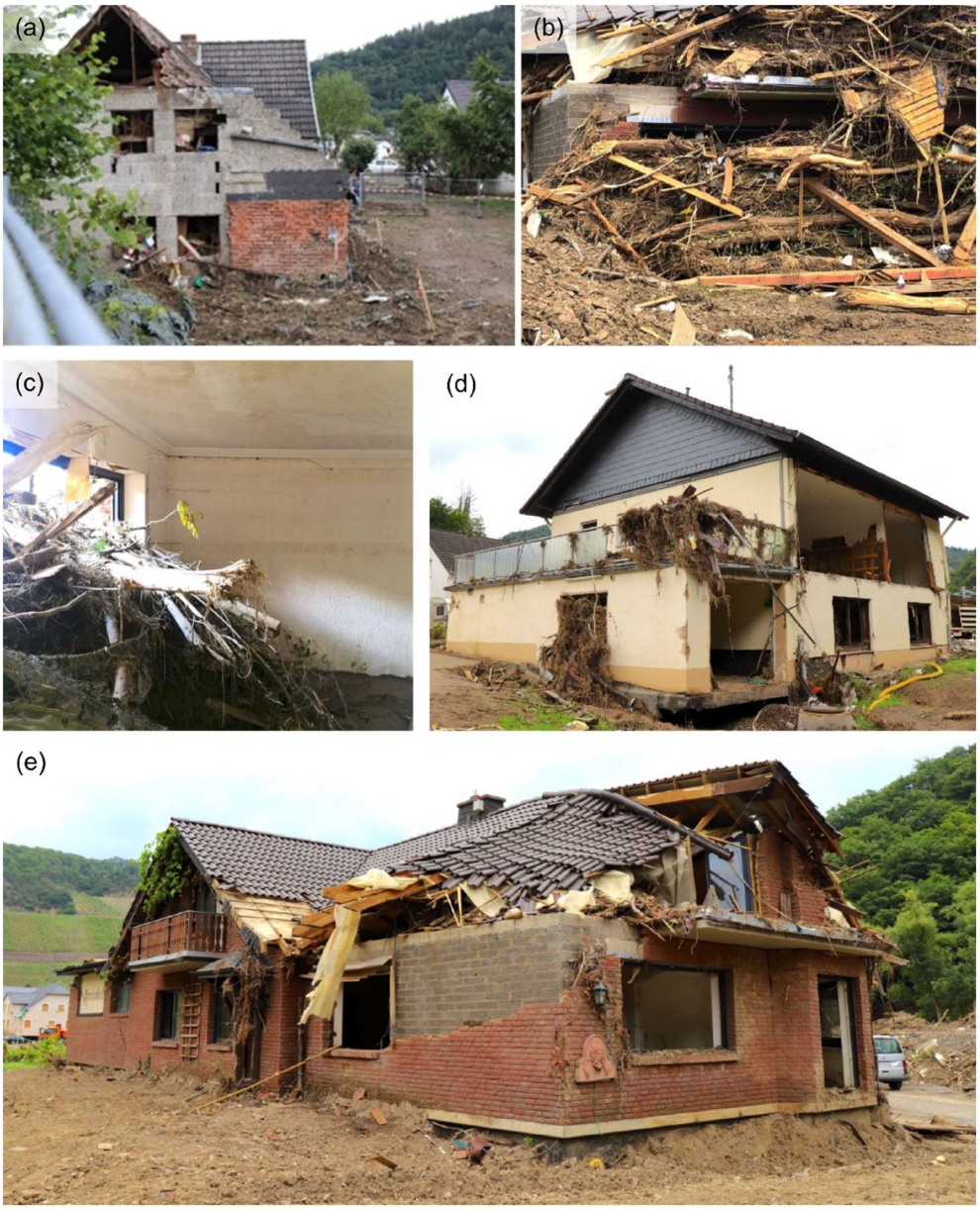

FIGURE 15 Photographs of remains of debris-dams accumulated at buildings. (a) Insul; (b, c, e) Dernau (same building); (d) Brück.

The survey showed that the structures most affected by debris-dams were located on the upstream end of each town. This is understandable since these structures acted as local debris collectors, therefore providing shelter to buildings located further downstream.

As an overly simplified example, Figure 16 shows the sketch of a house with its upstream side completely covered by debris, similar to those observed during the survey. Assume that the wall is 3 m tall, 6 m wide and that two windows of 1.5 m × 2 m are present at a height of 0.75 m. If the flood depth is 2 m and water flows through the openings, the area exposed to the flood is 8.25 m^2, which corresponds to a resultant hydrostatic pressure of 10γ (where γ is the specific weight of the water in N/m^3; Kelman & Spence, 2004). If the flow velocity is 1 m/s, the resultant hydrodynamic pressure, assuming a uniform distribution over the depth and a drag coefficient of 1.0 (Jansen et al., 2020), would be 8.25γ. When a debris dam builds up against the house, water can no longer flow freely through the openings, increasing the area exposed to the flow (Wüthrich et al., 2018). Moreover, the dam may also span out on the sides of the building, which further increases the obstructed area and therefore the loads. Besides, the reduced flow area may lead to a constriction of the flow depending on the neighbouring buildings and obstructions. This may lead to an increased water level in front of the house. For this example, the increase in water level is considered 10% and the additional area covered by the debris-dam on the sides of the building is assumed as 10% in total. This is an optimistic assumption since experiments have shown increases in water depth of up to 20%–25% depending on the flow

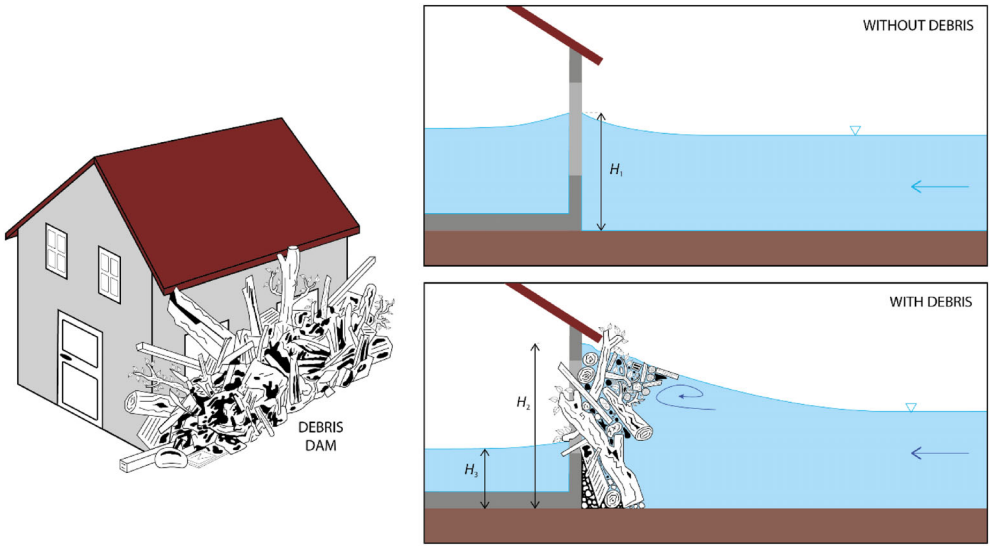

FIGURE 16 Sketch of 'debris-dam' resting on a building. Comparison of water levels with and without the dam.

conditions (Wüthrich, Ylla Arbós, et al., 2020). Ten percent increase means that the exposed area becomes 14 m^2 and corresponds to a resultant hydrostatic pressure of 16γ. If the flow velocity and drag coefficient remain unchanged, the hydrodynamic drag would amount to 14.5γ. Consequently, in this simple example, the debris dam leads to a 75% increase in the resultant hydrodynamic force exerted by the flood. Furthermore, the hydrostatic pressure is often equalised on both sides of the wall if water can enter the structure (Figure 16); but in the case of a debris dam, the water level inside could be lower than outside, which would add a hydrostatic component to this value.

The survey showed that some structures suffered from inwardly collapsed columns or walls. Discussions with local witnesses revealed that large amounts of debris had accumulated against these structures. At the time of the survey, many (partly) collapsed buildings had already been removed, so it is not possible to comment on the flood action that led to failure. However, Figure 17 presents two examples where flood loads, presumably related to debris, affected columns. The first case (Figure 17a–c), shows two missing columns temporarily supported with timber poles. The column on the leading edge (Figure 17b) was surrounded by flowing water which favoured debris collision. After the failure of the column, the debris accumulated inside the structure and pressed against the other two (Figure 17c), with the left one collapsing. The remaining column showed outwards out-of-plane deformation, while in Figure 17b the remaining column showed an inwards deformation. Similarly, in Figure 17d, the flood led to the partial collapse of a masonry wall, which tilted forward due to the flood actions acting primarily near its base. At the back of the house (Figure 17e), a column was removed by the flood which led to the partial collapse of the floor.

In summary, debris-damming is a natural process that induces additional flood loads that are rarely accounted for in river floods. Yet, the increased likelihood of collapse due to larger flood-induced forces should be considered in flood risk analyses, especially where large volumes of debris are available. Small debris, in large quantities, seems particularly dangerous in these types of floods.

5 | DISCUSSION AND RECOMMENDATIONS

The survey, conducted in the Ahr Valley one month after the July 2021 flood, was extremely helpful in providing first-hand information on the severe damages induced by this extreme event. While some buildings and rubble had already been removed at the time of this survey, these observations provided helpful information supporting a conscious assessment of the loads and failure mechanisms. In particular, this research provided some evidence on the failures associated with scour and bank erosion, hydraulic loads and floating debris. However, in reality, it is difficult to isolate processes that can occur simultaneously. Therefore, during the preliminary design, it is essential that expert judgement and simple structural analyses are used to identify most relevant failure mechanisms for a particular structure and a specific location.

Based on previous events, many criteria were developed to predict the collapse of buildings as a function of water level and flow velocity (e.g., Black, 1975; Maiwald & Schwarz, 2023; Sangrey et al., 1975;

FIGURE 17 Building damage associated with the failure of single elements: (a–c) failure of a pillar in Schuld, likely associated with the debris reported inside the structure (removed, hence not visible in the picture); (d) wall tilting forward and (e) cloumn missing at the corner in Insul. Red arrows indicate the suspected flow direction.

Smith, 1991). Recently, based on large-scale physical modelling, Jansen et al. (2020) formulated damage curves for typical Dutch masonry buildings during floods. For most building types, water depths larger than 1.5 m led to severe damage and even loss of stability. However, if water levels were equalised between the inside and outside of the houses, higher water depths of 2–2.5 m with flow velocities between 1.5 and 2.5 m/s were necessary to cause severe damage. Conversely, water depths of 1 m were evaluated to be similarly damaging if associated with high flow velocities around 4.5 m/s. The Clausen criteria (Clausen & Clark, 1990), which predicts collapse when water-depth $\times$ velocity $= 7\ m^2/s$, is slightly more optimistic. The observations gathered in this survey, together with numerical simulations of Apel et al. (2022), seem to confirm these criteria. While water depths were significant (up to 7.2 m), the water levels inside and outside of houses were often equalised, which means that damage mostly occurred for buildings affected by high flow velocities, often located close to wide streets and/or next to the river. Maiwald et al. (2022) also conducted a field study in the Ahr Valley and extended the existing EDAC (Earthquake Damage Analysis Center, Bauhaus University Weimar) flood database/flood damage model based on Maiwald and Schwarz (2023). More specifically, the study used the 2021 flood to improve the damage model, especially for high water levels and flow velocities (i.e., >4 m and >2 m/s), showing that the majority of masonry and timber-framed structures were damaged, while buildings with lower vulnerability (e.g., steel structures, reinforced concrete) were less affected, which is in agreement with the observations of the present field survey.

The survey also showed that damage and failure mechanisms must be analysed not only at building scale but also at town/city/village scale. This is because the interaction of the flood with irregularly distributed buildings led to spatially variable hydrodynamic conditions and, subsequently, to variable hydrodynamic loads acting on the buildings. This is particularly evident for buildings

located upstream of each village, which were often the most damaged (e.g., Figures 11b, 12b, and 15d,e) and the most affected by debris accumulation (e.g., Figure 12b). Similar observations were provided for tsunamis, where unshielded buildings near the shore are the most damaged (Moris et al., 2021; Pringgana et al., 2021). Similarly, for floods, Maiwald and Schwarz (2015) pointed out that the location of the building relative to the flow velocity vector (flow direction) and the urban integration had an influence on the structural damage, providing a simplified characterisation based on the arrangement of surrounding housing and flow characteristic. This highlights the importance of considering spatial planning as a tool to achieve community resilience and to limit building damage.

The heavy damages clearly pointed out the need for improved measures and regulations for reconstruction to avoid the '*rebuilding as it was*' approach. While the general advice is to avoid structures too close to the river or in flood-prone areas, some recommendations can be made based on this research:

- New constructions should favour the use of reinforced concrete, since it was shown to be less likely to fail, while structures built with wood or unreinforced masonry were more vulnerable to flood-induced loads.
- Revetment and pavements proved to be effective scour protection measures (Julien, 2002). These should be combined with deeper or piled foundations for buildings located near the river to combat bank erosion. Green infrastructures (i.e., grass and trees) were insufficient to prevent damage during this extreme event. Buildings at the extrados and intrados of river bends deserve particular attention.
- In line with Maiwald and Schwarz (2015), enhanced flood protection could be obtained through the development of spatial/land-use plans that include specific regulations favouring the construction of stronger buildings, which are specifically designed to shelter-others. These buildings could also have a more active role in collecting the floating debris transported by the flow, reducing the formation of debris-dams around downstream structures. Alternatively, debris could be collected/removed through racks and screens (Schalko et al., 2021), which is the approach used in dam-engineering to avoid driftwood accumulation at spillways. However, such an approach should be based on thorough political discussions and with a multi-disciplinary collaboration, including engineers, landscape designers and urban planners.

Despite the research conducted in the past, it is clear that the dynamics behind many of these processes still remain widely unknown, particularly those involving multiple phases (i.e., debris, sediments, air, fluid–structure interaction). More specifically, this survey showed that the behaviour of debris, their accumulation, backwater rise, induced loads and related scour-issues represent critical aspects that need to be addressed by researchers of all disciplines to develop reliable and effective flood protection measures. The spatial variation in water levels and the scour depths observed in the proximity of buildings further emphasise the need for more research to accurately assess flood loads.

6 | CONCLUSION

July 2021 was characterised by extreme floods in central Europe, with multiple casualties, severe damages and high economic losses. Particularly affected was the Ahr Valley (Germany), where in some areas (e.g., in Ahrbrück, see Figure 3a), water levels were 2.7 m higher than the previous maximum recorded flood in 1910. This paper reports the key observations and main results of a post-event field survey conducted by a team of hydraulic and structural engineers from The Netherlands and Germany. The objective of this research is to describe the flood-induced damage on buildings, assessing the possible underlying processes that led to structural failures. The survey focused on three main processes:

1. *Hydraulic loads*. The survey measured several water levels to determine the relevant flood-induced loads acting on buildings. Observations revealed that water inside the building neutralised the hydrostatic load, but hydrodynamic loads still occurred at considerable flow velocities. Particularly, unreinforced masonry and timber buildings suffered from significant damage, with the failure of the façades often affecting their structural integrity. Data also showed that the water levels were uneven around the four sides of buildings, confirming the temporal and spatial variability of the flow conditions, as well as the non-uniform distribution of loads acting on buildings during floods.
2. Flood-induced *scour* and *bank erosion*, which exposed and undermined the foundations of multiple buildings, stress the importance of protection measures, including pavements and revetments around buildings. The survey also pointed out the importance of deep foundations for buildings located near river bends, or in proximity of flow constrictions like bridges or other hydraulic structures.
3. Water-borne *debris* played a crucial role during the flood, with debris of different sizes and nature observed at multiple locations. Most common debris included driftwood, construction rubble and

sediments, but oil-tanks, cars, caravans and other man-made debris were also observed. These are relevant not only because they impacted and damaged vulnerable structures, but also because their heterogeneous nature facilitated entanglement and accumulation, creating large debris-dams upstream of buildings. This resulted in blocked openings, reduced water levels inside the buildings and backwater rise upstream, thus magnifying the area exposed to the flow. This increase in loads on buildings resulted in many structural failures, clearly visible during the survey. It follows that a strict debris-management plan will be fundamental in the future and that guidelines should be implemented to include debris damming as an important additional load.

Overall, the collected data and observations provided a better interpretation of the processes occurring during an extreme (flash) flood, with an insight on the most current failure mechanisms. It is also believed that these findings can stimulate future numerical and experimental studies on flood-related issues, which are necessary to better understand the physical behaviour of these natural hazards, supporting the development of safer flood protection measures. Altogether it is important to learn from past events, contributing to the plan to '*Build Back Better*'!

ACKNOWLEDGEMENTS

The authors would like to thank Ir. Roelof Moll (TU Delft) for his help in the organisation of this field survey. The support of Ms. Christiane Eichmanns and Dr. Stefanie Wolf on the second and third day of the survey is also acknowledged. The authors would like to further extend their thanks to Dr. Philipp Schulte (RWTH Aachen University) for providing us with the grain size information from the collected soil samples of the Ahr region. The authors would also like to thank Dr. Heiko Apel (GFZ-Potsdam) for sharing the numerical simulation data of the 2021 July flood event in Germany (Apel et al., 2022). Further the authors would like to thank the local citizens for welcoming us in their towns and showing them around, often sharing valuable information in support of this research. The contribution of Davide Wüthrich, Paul Korswagen and Jeremy Bricker was funded through a TKI Delta Technology project TU02 '*Building Collapse and Fatality During Floods*' The contribution of Harish Selvam and Jan Oetjen is funded in the frame of the '*Feasibility study for the assessment of the pollutant load of sediments as a result of the July flood 2021 in the transition from low mountain range to lowland*' (DFG Schu 1054/26-1). The financial contribution of the '*KAHR—Climate Adaptation, Flood, Resilience*' project is acknowledged. Open Access funding enabled and organized by Projekt DEAL.

CONFLICT OF INTEREST STATEMENT

The authors declare no conflict of interest.

DATA AVAILABILITY STATEMENT

Data presented in this study are available from the corresponding author upon reasonable request. All pictures and data are openly available at: https://doi.org/10.4121/19222656.

ORCID

Davide Wüthrich https://orcid.org/0000-0003-1974-3560
Paul A. Korswagen https://orcid.org/0000-0002-2587-7808
Harish Selvam https://orcid.org/0000-0002-6761-0562
Jan Oetjen https://orcid.org/0000-0002-3779-7020
Jeremy Bricker https://orcid.org/0000-0002-7503-6652
Holger Schüttrumpf https://orcid.org/0000-0002-0104-0499

ENDNOTES

[1] A '*disastrous*' flood is defined as a flood event which causes fatalities and disruption in society, included in the Emergency Events Database (EM-DAT; Guha-Sapir et al., 2022) or belongs to the group of 'large floods' in the Dartmouth Flood Observatory (DFO; Brakenridge, 2022).

[2] Note that these are local water depths related to the loads acting on individual buildings and do not correspond to the water level measured with the river's normal level as reference.

[3] According to Terzaghi (1943), the foundation is shallow if its depth is equal to or less than its width.

REFERENCES

Abernethy, B., & Rutherfurd, I. D. (1998). Where along a river's length will vegetation most effectively stabilise stream banks? *Geomorphology*, *23*, 55–75. https://doi.org/10.1016/S0169-555X(97)00089-5

Apel, H., Vorogushyn, S., & Merz, B. (2022). Brief communication: Impact forecasting could substantially improve the emergency management of deadly floods: Case study July 2021 floods in Germany. *Natural Hazards and Earth System Sciences*, *22*, 3005–3014. https://doi.org/10.5194/nhess-22-3005-2022

Arneson, L. A., Zevenbergen, L. W., Lagasse, P. F., & Clopper, P. E. (2012). *Evaluating scour at bridges (HEC-18)* (5th ed.). U.S. Department of Transportation Federal Highway Administration.

ASCE 7. (2017). Minimum design loads and associated criteria for buildings and other structures, Standards Ser, v.ASCE/SEI 7-16. American Society of Civil Engineers.

Bayón, A., Valero, D., & Franca, M. J. (2024). Urban flood drifters (UFD): Identification, classification and characterisation. *Journal of Flood Risk Management. Portico*. https://doi.org/10.1111/jfr3.13002

Bezzola, G. R., & Hegg, C. (2007). Ereignisanalyse Hochwasser 2005, Teil 1 – Prozesse, Schäden und erste Einordnung, Umwelt-Wissen, 0707, Bundesamt für Umwelt BAFU, Eidgenössische Forschungsanstalt WSL.

Black, R. D. (1975). *Floodproofing rural residences* (Washington D.C. Report no EDA 77-088). US Department of Commerce, Economic Development Administration.

Blöschl, G., Hall, J., Viglione, A., Perdigão, R. A. P., Parajka, J., Merz, B., Lun, D., Arheimer, B., Aronica, G. T., Bilibashi, A., Boháč, M., Bonacci, O., Borga, M., Čanjevac, I., Castellarin, A., Chirico, G. B., Claps, P., Frolova, N., Ganora, D., ... Živković, N. (2019). Changing climate both increases and decreases European river floods. *Nature*, *573*, 108–111. https://doi.org/10.1038/s41586-019-1495-6

Brakenridge, G. R. (2022). *Global active archive of large flood events, Dartmouth flood observatory*. University of Colorado. http://floodobservatory.colorado.edu/

Briaud, J.-L., Chen, H.-C., Chang, K.-A., Oh, S. J., Chen, S., Wang, J., Li, Y., & Kwak, K. (2011). *The SRICOS–EFA method: Summary report*.

Bricker, J. D., Francis, M., & Nakayama, A. (2012). Scour depths near coastal structures due to the 2011 Tohoku Tsunami. *Journal of Hydraulic Research*, *50*, 637–641. https://doi.org/10.1080/00221686.2012.721015

Bung, D. B. (2021). Extreme flooding in Western Germany: Some thoughts on hazards, return periods and risk. In *Hydrolink* (pp. 108–113). International Association for Hydro-Environment Engineering and Research.

Cantelmo, C., & Cuomo, G. (2021). Hydrodynamic loads on buildings in floods. *Journal of Hydraulic Research*, *59*, 61–74. https://doi.org/10.1080/00221686.2020.1714759

CEDIM. (2021). Hochwasser Mitteleuropa, Juli 2021 (Deutschland) 21. Juli 2021—Bericht Nr. 1 "Nordrhein-Westfalen & Rheinland-Pfalz". https://doi.org/10.5445/IR/1000135730

Chock, G., Carden, L., Robertson, I., Olsen, M., & Yu, G. (2013). Tohoku Tsunami-induced building failure analysis with implications for USA tsunami and seismic design codes. *Earthquake Spectra*, *29*, 99–126. https://doi.org/10.1193/1.4000113

Clausen, L., & Clark, P. B. (1990). The development of criteria for predicting dambreak flood damages using modelling of historical dam failures. In *Proceedings of the International Conference on River Flood Hydraulics* (pp. 369–380). John Wiley & Sons.

Dottori, F., Szewczyk, W., Ciscar, J.-C., Zhao, F., Alfieri, L., Hirabayashi, Y., Bianchi, A., Mongelli, I., Frieler, K., Betts, R. A., & Feyen, L. (2018). Increased human and economic losses from river flooding with anthropogenic warming. *Nature Climate Change*, *8*, 781–786. https://doi.org/10.1038/s41558-018-0257-z

FEMA. (2007). *Design guide for improving critical facility safety from flooding and high winds* (FEMA 543). Federal Emergency Management Agency.

Goseberg, N., Stolle, J., Nistor, I., & Shibayama, T. (2016). Experimental analysis of debris motion due the obstruction from fixed obstacles in tsunami-like flow conditions. *Coastal Engineering*, *118*, 35–49. https://doi.org/10.1016/j.coastaleng.2016.08.012

Gray, D. H., & Barker, D. (2004). Root-soil mechanics and interactions. In S. J. Bennett & A. Simon (Eds.), *Riparian vegetation and fluvial geomorphology* (pp. 113–123). American Geophysical Union. https://doi.org/10.1029/008WSA09

Guha-Sapir, D., Below, R., & Hoyois, P. (2022). *EM-DAT: The CRED/OFDA International Disaster database*. https://www.emdat.be/

Hager, W. H., & Unger, J. (2010). Bridge pier scour under flood waves. *Journal of Hydraulic Engineering*, *136*, 842–847. https://doi.org/10.1061/(ASCE)HY.1943-7900.0000281

Harish, S., Sriram, V., Schüttrumpf, H., & Sannasiraj, S. A. (2022a). Tsunami-like flow induced forces on the structure: Dependence of the hydrodynamic force coefficients on Froude number and flow channel width in quasi-steady flow phase. *Coastal Engineering*, *172*, 104078. https://doi.org/10.1016/j.coastaleng.2021.104078

Harish, S., Sriram, V., Schüttrumpf, H., & Sannasiraj, S. A. (2022b). Flow-structure interference effects with the surrounding structure in the choked quasi-steady condition of tsunami: Comparison with traditional obstruction approach. *Applied Ocean Research*, *126*, 103255. https://doi.org/10.1016/j.apor.2022.103255

Ikeno, M., Takabatake, D., Kihara, N., Kaida, H., Miyagawa, Y., & Shibayama, A. (2016). Improvement of collision force formula for woody debris by airborne and hydraulic experiments. *Coastal Engineering Journal*, *58*(4), 1640022. https://doi.org/10.1142/S0578563416400222

Jansen, L., Korswagen, P. A., Bricker, J. D., Pasterkamp, S., de Bruijn, K. M., & Jonkman, S. N. (2020). Experimental determination of pressure coefficients for flood loading of walls of Dutch terraced houses. *Engineering Structures*, *216*, 110647. https://doi.org/10.1016/j.engstruct.2020.110647

Julien, P. Y. (2002). *River mechanics*. Cambridge University Press. https://doi.org/10.1017/CBO9781139164016

Junghänel, T., Bissolli, P., Daßler, J., Fleckenstein, R., Imbery, F., Janssen, W., Kaspar, F., Lengfeld, K., Leppelt, T., Rauthe, M., Rauthe-Schöch, A., Rocek, M., Walawender, E., & Weigl, E. (2021). Hydro-klimatologische Einordnung der Stark-und Dauerniederschläge in Teilen Deutschlands im Zusammenhang mit dem Tiefdruckgebiet "Bernd" vom 12 bis 19 Juli 2021.

Kelman, I., & Spence, R. (2004). An overview of flood actions on buildings. *Engineering Geology*, *73*, 297–309. https://doi.org/10.1016/j.enggeo.2004.01.010

Kohli, A., & Hager, W. H. (2001). Building scour in floodplains, proceedings of the Institution of Civil Engineers - water and maritime. *Engineering*, *148*, 61–80. https://doi.org/10.1680/wame.2001.148.2.61

Koks, E., van Ginkel, K., van Marle, M., & Lemnitzer, A. (2022). Brief communication: Critical infrastructure impacts of the 2021 mid-July western European flood event. *Natural Hazards and Earth System Sciences*, *22*(12), 3831–3838. https://doi.org/10.5194/nhess-2021-394

Korswagen, P. A. (2016). *Structural damage to masonry housing due to earthquake-flood multi-hazards*. MSc. Thesis. TU Delft.

Korswagen, P. A., Harish, S., Oetjen, J., & Wüthrich, D. (2022). *Post-flood field survey of the Ahr Valley (Germany): Building damages and hydraulic aspects* (TU Delft Report 69). Delft University of Technology. https://doi.org/10.4121/19222656

Kothayari, U. C., Garde, R. C. J., & Ranga Raju, K. G. (1992). Temporal variation of scour around circular bridge piers. *Journal of Hydraulic Engineering*, *118*, 1091–1106. https://doi.org/10.1061/(ASCE)0733-9429(1992)118:8(1091)

Krautwald, C., Stolle, J., Robertson, I., Achiari, H., Mikami, T., Nakamura, R., Takabatake, T., Nishida, Y., Shibayama, T.,

Esteban, M., Goseberg, N., & Nistor, I. (2021). Engineering lessons from September 28, 2018 Indonesian tsunami: Scouring mechanisms and effects on infrastructure. *Journal of Waterway, Port, Coastal, and Ocean Engineering*, *147*, 04020056. https://doi.org/10.1061/(ASCE)WW.1943-5460.0000620

Kundzewicz, Z. W., Pisnkwar, I., & Brakenridge, G. R. (2018). Changes in river flood hazard in Europe: A review. *Hydrology Research*, *49*(2), 294–302. https://doi.org/10.2166/nh.2017.016

Laudan, J., Rözer, V., Sieg, T., Vogel, K., & Thieken, A. H. (2017). Damage assessment in Braunsbach 2016: Data collection and analysis for an improved understanding of damaging processes during flash floods. *Natural Hazards and Earth System Sciences*, *17*(12), 2163–2179. https://doi.org/10.5194/nhess-17-2163-2017

Lee, S. O., & Hong, S. H. (2019). Turbulence characteristics before and after scour upstream of a scaled-down bridge pier model. *Water*, *11*, 1900. https://doi.org/10.3390/w11091900

Li, Y., Briaud, J.-L., Chen, H.-C., Nurtjahyo, P., & Wang, J. (2002). Shallow water effect on pier scour in Clays, College Station, Texas: Texas Transportation Inst., Publications Dept., First International Conference on Scour of Foundations.

Maiwald, H., & Schwarz, J. (2015). Damage and loss prognosis tools correlating flood action and building's resistance-type parameters. *International Journal of Safety and Security Engineering*, *5*(3), 222–250. https://doi.org/10.2495/SAFE-V5-N3-222-250

Maiwald, H., & Schwarz, J. (2023). Ermittlung von Hochwasserschäden unter Berücksichtigung der Bauwerksverletzbarkeit, Erweitertes EDAC-Hochwasserschadensmodell, scientific technical reports 01-22, Zentrum für die Ingenieuranalyse von Erdbebenschäden, Bauhaus-Universitätsverlag.

Maiwald, H., Schwarz, J., Kaufmann, C., & Abrahamczyk, L. (2022). Das Hochwasser 2021—Ingenieuranalyse der Bauwerksschäden. *Bautechnik*, *99*(12), 878–890. https://doi.org/10.1002/bate.202200062

Matsutomi, H. (2009). Method for estimating collision force of driftwood accompanying tsunami inundation flow. *Journal of Disaster Research*, *4*(6), 435–440. https://doi.org/10.20965/jdr.2009.p0435

Mehrzad, R., Nistor, I., & Rennie, C. (2022). Scour mechanics of a tsunami-like bore around a square structure. *Journal of Waterway, Port, Coastal, and Ocean Engineering*, *148*, 04021048. https://doi.org/10.1061/(ASCE)WW.1943-5460.0000686

Melville, B. W. (1997). Pier and abutment scour: Integrated approach. *Journal of Hydraulic Engineering*, *123*, 125–136. https://doi.org/10.1061/(ASCE)0733-9429(1997)123:2(125)

Melville, B. W., & Raudkivi, A. J. (1977). Flow characteristics in local scour at bridge piers. *Journal of Hydraulic Research*, *15*, 373–380. https://doi.org/10.1080/00221687709499641

Merz, B., Blöschl, G., Vorogushyn, S., Dottori, F., Aerts, J. C. J. H., Bates, P., Bertola, M., Kemter, M., Kreibich, H., Lall, U., & Macdonald, E. (2021). Causes, impacts and patterns of disastrous river floods. *Nature Reviews Earth and Environment*, *2*, 592–609. https://doi.org/10.1038/s43017-021-00195-3

MKUEM. (2023). Die Ahr, Ministerium für Klimaschutz, Umwelt, Energie und Mobilität Rheinland-Pfalz. https://wasser.rlp-umwelt.de/servlet/is/1210/#:~:text=Die%20Ahr%20entw%C3%A4ssert%20ein%20Niederschlagseinzugsgebiet,Adenauer%20Bach%20und%20Staffeler%20Bach

Möller, H. (2020). Kleinod. https://www.google.com/maps/place/Kleinod/@50.5326618,7.0625751,3a,75y,90t/data=!3m8!1e2!3m6!1sAF1QipOdbxArfevYDARGNlA1yRX0PDcfXBVWioJJufoy!2e10!3e12!6shttps:%2F%2Flh5.googleusercontent.com%2Fp%2FAF1QipOdbxArfevYDARGNlA1yRX0PDcfXBVWioJJufoy%3Dw203-h152-kno!7i4000!8i3000!4m17!1m9!3m8!1s0x47befe88d63cb521:0xa22d4d79d2bd150!2sDernau-Marienthal!3b1!8m2!3d50.5353987!4d7.0585868!10e5!16s%2Fg%2F1226sb2g!3m6!1s0x47befe8dd9c77c2b:0x2639fd2fae7ebf8c!8m2!3d50.5326713!4d7.062574!10e5!16s%2Fg%2F11bbt3x18f?entry=ttu

Moris, J. P., Kennedy, A. B., & Westerink, J. J. (2021). Tsunami wave run-up load reduction inside a building array. *Coastal Engineering*, *169*, 103910. https://doi.org/10.1016/j.coastaleng.2021.103910

Munich Re. (2022). Hurricanes, cold waves, tornadoes: Weather disasters in USA dominate natural disaster losses in 2021. https://www.munichre.com/en/company/media-relations/media-information-and-corporate-news/media-information/2022/natural-disaster-losses-2021.html

Nadal, N. C., Zapata, R. E., Pagán, I., López, R., & Agudelo, J. (2010). Building damage due to riverine and coastal floods. *Journal of Water Resources Planning and Management*, *136*, 327–336. https://doi.org/10.1061/(ASCE)WR.1943-5452.0000036

Nistor, I., Goseberg, N., & Stolle, J. (2017). Tsunami-driven debris motion and loads: A critical review. *Frontiers in Built Environment*, *3*, 2. https://doi.org/10.3389/fbuil.2017.00002

OpenTopoMap. (2021). OpenStreetMap, SRTM. https://opentopomap.org

Paulik, R., Crowley, K., & Williams, S. (2021). *Post-event flood damage surveys: A New Zealand experience and implications for flood risk analysis*. Science and practice for an uncertain future.

Pringgana, G., Cunningham, L. S., & Rogers, B. D. (2021). Influence of orientation and arrangement of structures on tsunami impact forces: Numerical investigation with smoothed particle hydrodynamics. *Journal of Waterway, Port, Coastal, and Ocean Engineering*, *147*(3), 04021006. https://doi.org/10.1061/(ASCE)WW.1943-5460.0000629

Richardson, E. V., & Davis, S. R. (2001). *Evaluating scour at bridges (HEC-18)* (4th ed.). U.S. Department of Transportation Federal Highway Administration.

Roggenkamp, T., & Herget, J. (2014). Reconstructing peak discharges of historic floods of the river Ahr. *Germany, Erdkunde*, *68*, 49–59. https://doi.org/10.3112/erdkunde

Roggenkamp, T., & Herget, J. (2022). Projektbericht—Hochwasser der Ahr im Juli 2021—Abflussabschätzung und Einordnung. HW—Hydrologische Notizen, 66.

Rueben, M., Cox, D., Holman, R., Shin, S., & Stanley, J. (2015). Optical measurements of tsunami inundation and debris movement in a large-scale wave basin. *Journal of Waterway, Port, Coastal, and Ocean Engineering*, *141*(1), 04014029. https://doi.org/10.1061/(ASCE)WW.1943-5460.0000267

Sangrey, D. A., Murphy, P. J., & Nieber, J. L. (1975). Evaluating the impact of structurally interrupted flood plain flows, Cornell University. Prepared for: Office of Water Research and Technology.

Schalko, I., Ruiz-Villanueva, V., Maager, F., & Weitbrecht, V. (2021). Wood retention at inclined Bar screens: Effect of wood characteristics on backwater rise and bedload transport. *Water*, *13*(16), 2231. https://doi.org/10.3390/w13162231

Schmocker, L., & Hager, W. H. (2013). Scale modeling of wooden debris accumulation at a debris rack. *Journal of Hydraulic*

Engineering, *139*(8), 827–836. https://doi.org/10.1061/(ASCE)HY.1943-7900.0000714

Schwarz, J., & Maiwald, H. (2007). Prognose der Bauwerksschädigung unter Hochwassereinwirkung. *Bautechnik*, *84*, 450–464. https://doi.org/10.1002/bate.200710039

Smith, D. I. (1991). Extreme floods and dam failure inundation implications for loss assessment. Proceedings of a seminar Natural and Technological Hazards: Implications for the Insurance Industry.

Sonia Devi, Y., & Barbhuiya, A. K. (2017). Bridge pier scour in cohesive soil: A review. *Sādhanā*, *42*, 1803–1819. https://doi.org/10.1007/s12046-017-0698-5

Stolle, J., Takabatake, T., Nistor, I., Mikami, T., Nishizaki, S., Hamano, G., Ishii, H., Shibayama, T., Goseberg, N., & Petriu, E. (2018). Experimental investigation of debris damming loads under transient supercritical flow conditions. *Coastal Engineering*, *139*, 16–31. https://doi.org/10.1016/j.coastaleng.2018.04.026

Sundar, V., Sannasiraj, S. A., Murali, K., & Sundaravadivelu, R. (2007). Runup and inundation along the Indian peninsula, including the Andaman Islands, due to great Indian Ocean tsunami. *Journal of Waterway, Port, Coastal, and Ocean Engineering*, *133*, 401–413. https://doi.org/10.1061/(ASCE)0733-950X(2007)133:6(401)

Terzaghi, K. (1943). *Theoretical soil mechanics*. John Wiley & Sons. https://doi.org/10.1002/9780470172766

Thieken, A. H., Bubeck, P., Heidenreich, A., von Keyserlingk, J., Dillenardt, L., & Otto, A. (2023). Performance of the flood warning system in Germany in July 2021—Insights from affected residents. *Natural Hazards and Earth System Sciences*, *23*, 973–990. https://doi.org/10.5194/nhess-23-973-2023

Ulrich, C. (1938). Hochwasserkatastrophe der Ahr am 12./13. Juni 1910, Jahrbuch des Kreises Ahrweiler, 92–106.

UNDRR. (2015). *Making development sustainable: The future of disaster risk management, global assessment report on disaster risk reduction*.

Unger, J., & Hager, W. H. (2006). Down-flow and horseshoe vortex characteristics of sediment embedded bridge piers. *Experiments in Fluids*, *42*, 1–19. https://doi.org/10.1007/s00348-006-0209-7

Vorogushyn, S., Apel, H., Kemter, M., & Thieken, A. H. (2022). Analyse der Hochwassergefährdung Im Ahrtal Unter Berücksichtigung historischer Hochwasser. *Fachartikel*, *66*, 244–254. https://doi.org/10.5675/HyWa_2022.5_2

Widiyanto, W., Santoso, P. B., Hsiao, S.-C., & Imananta, R. T. (2019). Post-event field survey of 28 September 2018 Sulawesi earthquake and tsunami. *Natural Hazards and Earth System Sciences*, *19*, 2781–2794. https://doi.org/10.5194/nhess-19-2781-2019

Wu, B., & Molinas, A. (2005). Energy losses and threshold conditions for choking in channel contractions. *Journal of Hydraulic Research*, *43*, 139–148. https://doi.org/10.1080/00221686.2005.9641230

Wüthrich, D., Pfister, M., Nistor, I., & Schleiss, A. J. (2018). Experimental study on forces exerted on buildings with openings due to extreme hydrodynamic events. *Coastal Engineering*, *140*, 72–86. https://doi.org/10.1016/j.coastaleng.2018.06.002

Wüthrich, D., Pfister, M., & Schleiss, A. J. (2020). Forces on buildings with openings and orientation in a steady post-tsunami free-surface flow. *Coastal Engineering*, *161*, 103753. https://doi.org/10.1016/j.coastaleng.2020.103753

Wüthrich, D., Ylla Arbós, C., Pfister, M., & Schleiss, A. J. (2020). Effect of debris damming on wave-induced hydrodynamic loads against free-standing buildings with openings. *Journal of Waterway, Port, Coastal, and Ocean Engineering*, *146*, 04019036. https://doi.org/10.1061/(ASCE)WW.1943-5460.0000541

Zevenbergen, L. W., Lagasse, P. F., & Edge, B. L. (2004). *Tidal hydrology, hydraulics and bridge scour* (Vol. 25). Federal Highway Agency, National Highway Institute. Hydraulic Engineering Circular.

Zhu, H., Hu, X., Li, Z., Song, L., Li, K., Li, X., & Li, G. (2018). The influences of riparian vegetation on bank failures of a small meadow-type Meandering River. *Water*, *10*, 692. https://doi.org/10.3390/w10060692

SUPPORTING INFORMATION

Additional supporting information can be found online in the Supporting Information section at the end of this article.

How to cite this article: Wüthrich, D., Korswagen, P. A., Selvam, H., Oetjen, J., Bricker, J., & Schüttrumpf, H. (2024). Field survey assessment of flood loads and related building damage from the July 2021 event in the Ahr Valley (Germany). *Journal of Flood Risk Management*, e13024. https://doi.org/10.1111/jfr3.13024